ASSESSMENT OF INTERFEROMETRIC SAR-BASED DIGITAL ELEVATION MODELS

Yen-Yi Wu (1, 2), Shih-Yuan Lin (2), Hsuan Ren (1)

[1] National Central University, No. 300, Zhongda Rd., Zhongli District, Taoyuan City 32001, Taiwan
[2] National Chengchi University, No. 64. Sec.2, Zhi-Nan Rd, Wenshan District, Taipei City 11605, Taiwan
Email: 108022004@cc.ncu.edu.tw; syl@nccu.edu.tw; hren@csrsr.ncu.edu.tw

KEY WORDS: InSAR, Digital Elevation Model, Seasonal effects, Multi-look processing, DEM accuracy

ABSTRACT: Interferometric Synthetic Aperture Radar (InSAR) is an established technique to extract 3D information of surfaces by using SAR images. InSAR techniques provide the capability to detect surface deformation and to generate Digital Elevation Models (DEM). However, while the methodology is well-established, it remains challenging to produce convincing InSAR DEM over vegetated areas due to temporal decorrelation. In order to address the issue, we aim at improving the quality of InSAR DEM by selecting appropriate datasets in the pre-processing stage, and by systematically assessing parameter variations during processing, especially for vegetated areas. Using C-band Sentinel-1A and Sentinel-1B satellite images, the test has been conducted over the Taichung area of Taiwan, where images cover both urban and vegetated areas. Winter and summer datasets are applied to observe seasonal effects. Besides, a multi-look processing procedure is carried out to inspect the influence of this process. Our experimental results demonstrate that winter datasets outperform summer datasets, achieving up to 13 meters of Root Mean Square Error (RMSE) in urban areas. It is also noted that multi-look processing procedure has different effects in our results; it improves the result for the summer pair but reduces the accuracy for the winter pair. In addition, one common property for both seasonal effects and multi-look processing effects is that the processing has more evident impact over higher elevated vegetated terrain than plane urban areas. To conclude, selecting datasets of appropriate season, and deciding if applying a multi-look processing procedure based on the property of datasets could improve the reliability of InSAR DEMS.

1. INTRODUCTION

InSAR has been extensively used for decades to extract 3D information of a surface by using phase information of SAR images obtained by radar antennas under different timing covering the same ground location. InSAR techniques provide the capability to detect surface deformation (Massonnet et al., 1993; Murakami et al., 1996; Peltzer and Rosen, 1995; Zebker et al., 1994a) and to generate Digital Elevation Models (DEM). While there are various ways to obtain DEMs, techniques other than InSAR are usually limited to provide results with the latest datasets within a short time, which is a problem when rapid response decision have to be made. Thus timeliness is one of the advantage of the InSAR technique over other techniques. However, while the methodology is well-established, it remains challenging to produce convincing InSAR results over vegetated areas due to temporal and geometric decorrelation. Temporal decorrelation occurs when canopy changes significantly between the temporal baselines. It has been shown that the temporal variation of backscattering for surface changes leads to loss of InSAR coherence (Li and Goldstein, 1990; Rodriguez and Martin, 1992; Zebker and Villasenor, 1992; Zebker et al., 1994b). Geometric decorrelation results from the distance between satellite positions during acquisition. Due to the change of observation angles, the correlation of the signals will be reduced. It leads to the loss of coherence as well (Zebker and Villasenor, 1992; Hanssen, 2001). This decorrelation remains an issue for obtaining plausible InSAR products, especially for vegetated and higher elevated terrains. As a result, improving the quality of InSAR DEM over vegetated and higher elevation areas is a necessary task to be addressed.

In our previous research (Wu and Lin, 2019), we composed a pair from two C-band Sentinel-1A. The main goal was to observe the seasonal effect on the InSAR DEM results, as well as to observe the relationship between elevation and RMSE of InSAR DEM. Our previous work suggested that the winter pairs provide better results than summer pair images, and also showed a positive relationship between elevation and RMSE. Since there are several demerits in the original setting, and other factors also need to be considered besides seasonal effects, a number of settings were further refined in the extended research. First of all, in our previous research, the perpendicular baseline of winter and summer pair data were 140.84 meters and 8.75 meters respectively, which theoretically contributes to inferior summer pair results, as a shorter baseline deteriorates the InSAR's sensitivity to height variation (ESA, 2007). Secondly, the temporal baselines were 12 days for both seasonal pairs. This is one of the factors that produced more pronounced effects in our results in vegetated areas than urban areas. Thirdly, using only one test area to conclude seasonal effects was not convincing. Fourthly, in the assessment part of our previous research, only 30 checkpoints were selected for each subset, which was not enough for establishing reliable

statistics. Therefore, this research copes with the issues and implements the following changes: (1) similar perpendicular baselines for each seasonal pair were carefully chosen to minimize the effect of various perpendicular baselines; (2) for the sake of mitigating the impact of temporal decorrelation, one Sentinel-1A and one Sentinel-1B satellite dataset are selected for both winter and summer image pairs to build a 6-day temporal baseline pair; (3) Taichung City is selected as test site to verify previously made conclusions; (4) checkpoints are increased to 10,000 for each subset to ensure reliable RMSE statistics.

The ESA SNAP software is used to generate DEMs. To that end, a workflow of procedures are necessary to be carried out. Among all of the steps, multi-look processing is an optional procedure. The purpose of multi-look processing and filter processing is to reduce inherent phase noise in SAR processing. However, since there is a risk of degrading image resolution if applying multi-look processing, and moreover, it does not guarantee a better accuracy, the multi-look processing procedure is often skipped when generating InSAR DEMs. As a result, the other goal of this research is to discuss the influence of multi-look processing for InSAR processing. In the assessment part, a referenced LiDAR DEM is used to verify the accuracy of InSAR DEMs.

2. TEST SITE AND DATA

2.1 Test Site

In this paper, a subset of Taichung City is chosen as the study area to provide a comparison with previous work. The geographical coordinates ranges from 24°4′18.44″ to 24°16′18.54″ North and 120°38′51.69″ to 120°47′39.8″ East. The large subset of Taichung City is divided into three smaller subsets A, B and C equally in Figure 1. The elevation is low (~50 m above sea level) in the west and high (~600 meters above sea level) in the east. The main land cover is characterized by urban areas and vegetated hills.

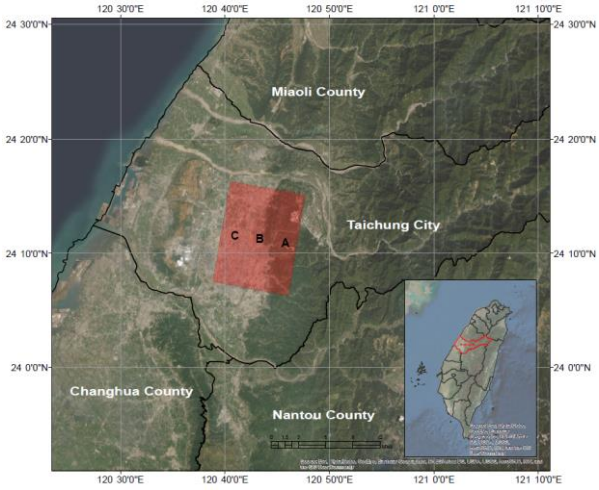

Figure 1 Test site area (ESRI basemap)

2.2 Data Source

Sentinel-1A and Sentinel-1B images in interferometric wide (IW) swath mode have range resolutions of 2.7-3.5 meters and an azimuth resolution of 22 meters. In order to reach a 6-day temporal baseline, the combination of one 1A image and one 1B image were selected as a pair. One pair for both winter and summer over experimental area was required. The detailed geometric parameters information is shown in Table 1.

Table 1 Geometric parameters of data

	Winter		*Summer*	
Satellite	S1B	S1A	S1A	S1B
Master/Slave	Master	Slave	Master	Slave
Date	2018.12.08	2018.12.14	2019.06.12	2019.06.18
Track	105	105	105	105
Orbit	13956	25027	27652	16756
Perpendicular Baseline (m)	0.00	141.83	0.00	144.20
Temporal Baseline (days)	0.00	6	0.00	6

Modeled Coherence	1.00	0.87	1.00	0.87
Height Ambiguity (m)	∞	-110.02	∞	-108.23
Averaged Incidence Angle (°)	43.7070	43.7141	43.7204	43.7118

3. RESEARCH METHODS

3.1 Workflow

The ESA SNAP software package is employed to generate DEMs in this research. One SLC master product and one SLC slave product are selected as a pair. The workflow is shown in Figure 2. This process includes steps such as coregistration, interferogram, deburst, subsetting, filtering, unwrapping, phase to elevation and range-doppler correction are necessary steps, while multilooking is an optional step, indicated by a dashed box in Figure 2. Multi-look processing could be conducted either before or after filter processing. In our experiment, it was processed before filter processing.

Since there is no package in the SNAP software for performing unwrapping, so the third-party software, SNAPHU, is utilized. A number of steps like coregistration, phase to elevation and range-doppler correction need a referenced DEM for supplementing geometric information. In this research, a 20 meters resolution LiDAR DEM is applied as the referenced DEM. In the accuracy assessment, the same LiDAR DEM is used to verify the accuracy of output InSAR DEMs.

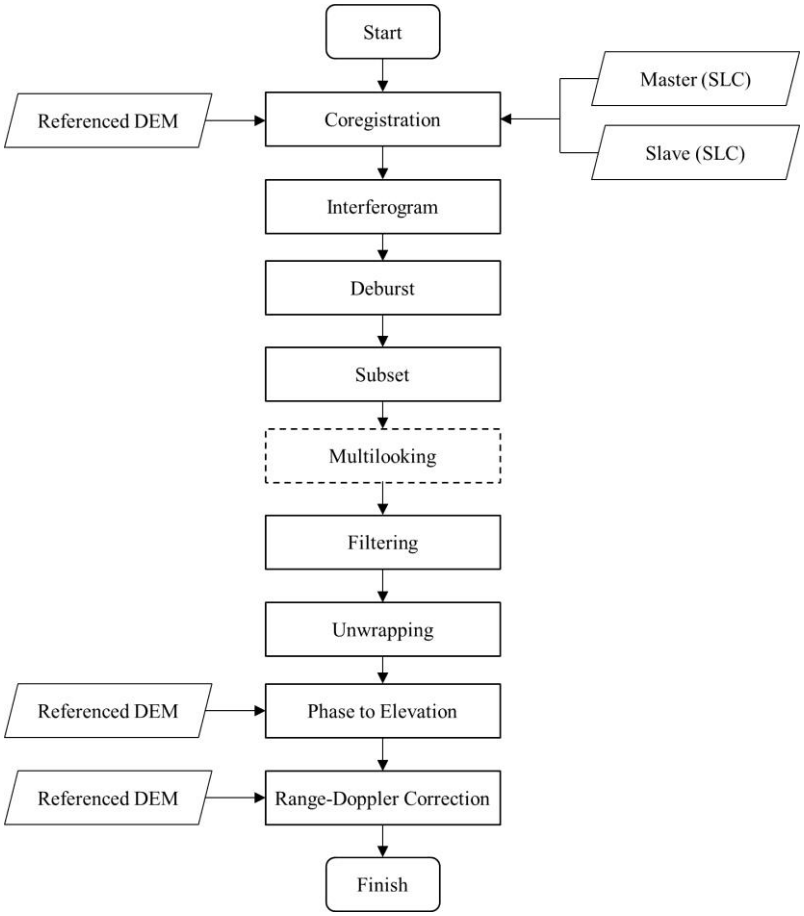

Figure 2 Workflow for developing an InSAR DEM

3.2 Multi-look Processing

Radar images contain inherent speckle noises, which degrades the quality of radar images and renders it difficult to interpret and inspect the main features. Speckle noises appear in a form of “grainy salt and pepper” due to interference patterns in the scattering process (ESA, 2019). In order to reduce the effect and increase signal-to-noise ratio, filtering and multi-look processing procedures are conducted.

The principle of multi-look processing is to divide the radar beam into several narrower sub-beams. Each sub-beam provides different and independent "looks" at the illuminated scene. The different looks are averaged to smooth out the speckle. Nevertheless, while the speckle variance is mitigated, the resolution (or pixel size) is degraded on the other side (ESA, 2019). All in all, due to the decrease of resolution, multi-look processing does not promise a better result in the end. As a result, in many TOPSAR tutorials (e.g. ESA, 2016; UAF, 2018), multi-look processing is usually skipped.

Because there is a trade-off between speckle noises and resolution, it is difficult to judge if multi-look processing is beneficial in a situation. Thus, in order to observe the effect of multi-look processing, each pair will be processed with and without multi-look procedure. In the following texts, the pair for which a multi-look processing is conducted is noted as "w/ ML", and the pair without application of multi-look processing is noted as "w/o ML". Table 2 illustrates the ratio of looks and their influence under each circumstance. The original azimuth spacing and range spacing are 13.97 meters and 2.33 meters, which results in a 13.97 m pixel size. In our research, 2:6 is applied as the ratio for azimuth looks and range looks, and the resolution of w/ ML pair will reach 27.94 meters.

Table 2 Multi-look (ML) processing information

	w/o ML	*w/ ML*
Azimuth spacing (m)	13.97	27.94
Range spacing (m)	2.33	13.98
Azimuth looks	1	2
Range looks	1	6
Pixel size (m)	13.97	27.94

3.3 Subset

To observe the difference between land elevation and land cover, the original image is divided into three subsets, which hereinafter are referred to as subset A, B and C. The size of each subset is about 1170 pixels.

Figure 3 (left) displays elevation data for the subsets, based on a 20 meters LiDAR DEM as background. The elevation height ranges from 46 to 634 meters above sea level. Subset A has the highest mean elevation, and it gradually lowers from A to C. (Table 3)

Figure 3 (right) displays the land cover of the subsets, with the ESRI World Imagery Basemap as background. Subset A covers more vegetated areas while subset C covers more urban areas.

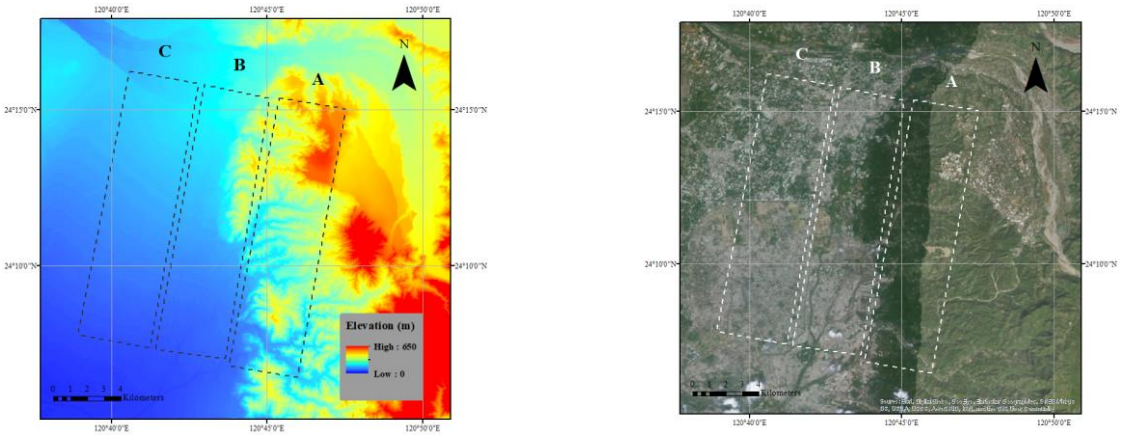

Figure 3 Areas of subset A, B and C over the LiDAR DEM (left) and World Imagery Basemap (right)

Table 3 Elevation Statistics of the test sites (in meters)

	Whole	*Subset A*	*Subset B*	*Subset C*
highest	634	634	505	209
lowest	46	78	55	46
mean	206.365	319.264	171.971	129.866
standard deviation	122.356	127.905	84.684	42.890

4. RESULTS

4.1 InSAR DEM Results

Figure 5 illustrates the results of the InSAR generated DEM. Subfigure I is the referenced LiDAR DEM, which is considered as reference value in our research. Subfigures II to V show the results of different pairs. Subset B and subset C of subfigure II to V show lower elevation values (indicated as blue) and resemble the referenced DEM (subfigure I). In contrast, subset A of subfigure II to V yields unstable and various results in comparison to the referenced DEM, because the area is characterized by vegetation canopy and the elevation is higher. This implies that the major significant differences between each result lies in subset A.

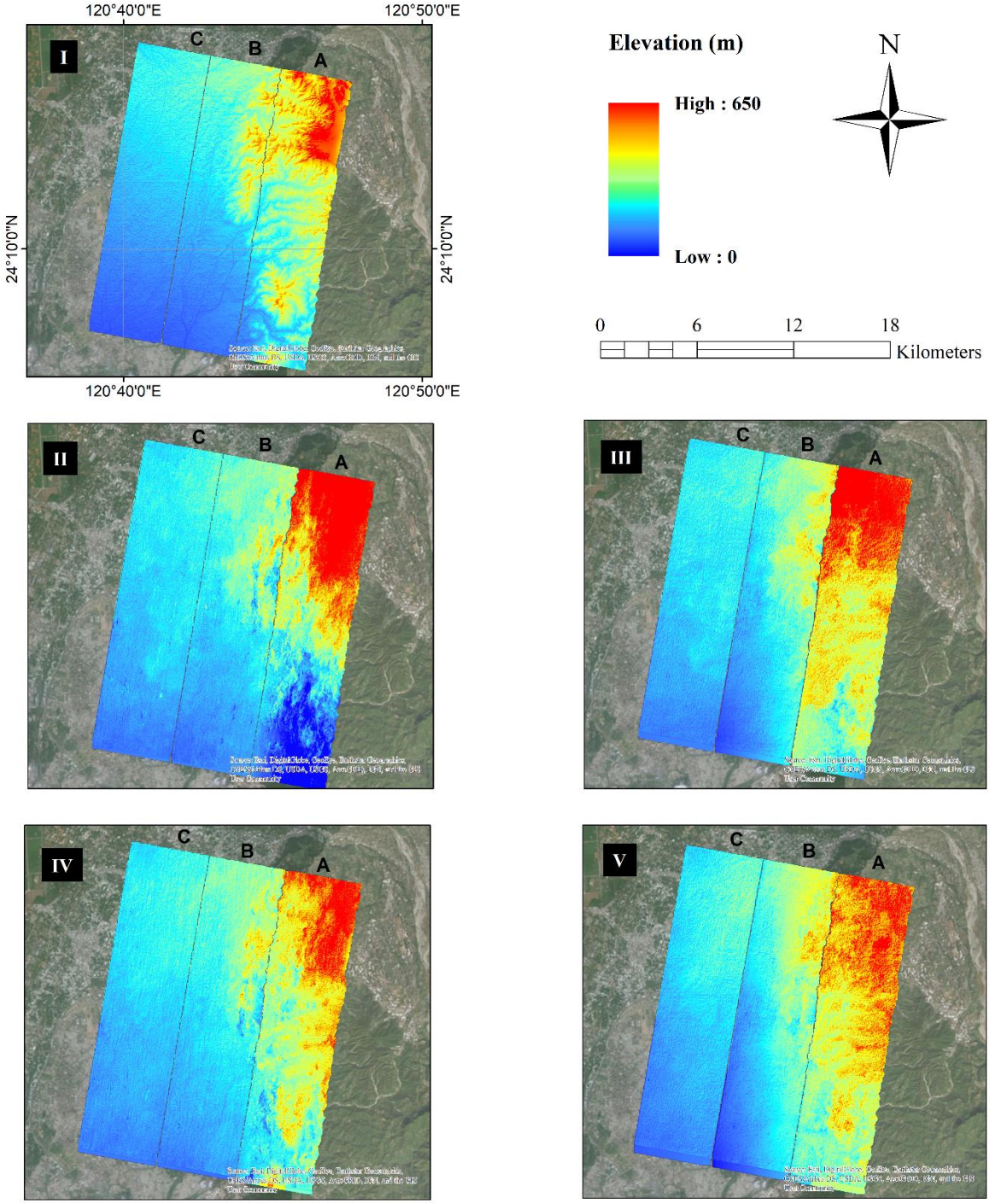

Figure 4 Results of InSAR DEM generation (subfigure I is a referenced LiDAR DEM, subfigure II is a summer pair w/o ML, subfigure III is a summer pair w/ ML, subfigure IV is a winter pair w/o ML, subfigure V is a winter pair w/ ML)

4.2 Difference

The elevation generated by the InSAR processing is ellipsoidal heights (h), which need to be transformed into orthometric heights (H) in order to compare the outputs with referenced DEM. This transformation is calculated using the information of undulation (N). The geometrical relationship of ellipsoidal heights (h), orthometric heights (H) and undulation (N) is seen as Eq. (1) (Kavoglu and Saka, 2005).

$$H = h - N \quad (1)$$

The undulation model applied in this research was published by The Ministry of the Interior in Taiwan in 2016 (National Development Council, 2016). Figure 5 shows the undulation of the test site. The undulation value is larger in the East and smaller in the West, ranging from 19.55 to 20.74 meters.

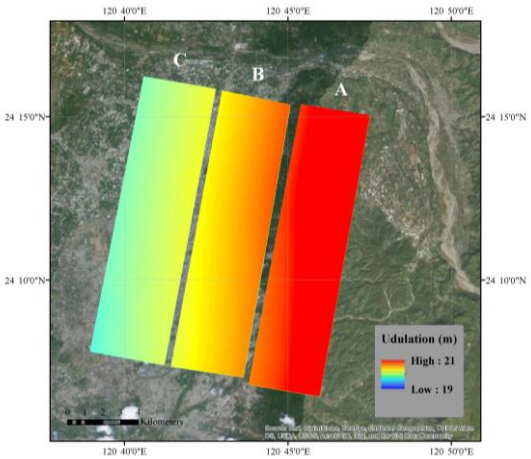

Figure 5 Undulation of the test site

With the orthometric heights of the InSAR DEM, the difference value could be derived by Eq. (2). Where H_{InSAR} represents the orthometric heights of InSAR DEM, H_{DEM} represents the orthometric heights of referenced DEM, and Δh represents the difference of InSAR DEM and referenced DEM.

$$\Delta h = H_{InSAR} - H_{DEM} \quad (2)$$

4.2.1 Qualitative Analysis

After applying Eq. (1) and Eq. (2) to InSAR DEM, the difference between the InSAR and referenced DEM is calculated. In Figure 6, subfigure I is the referenced LiDAR DEM, shown to demonstrate the relationship between elevation and difference. Subfigures II to V are the difference results for each pair. From Figure 6, several observations can be made: (1) in subset C, where the elevation is relatively low and land cover is mostly urban, a tilt pattern appears in each pair, showing subtle blue to red colors from north to south. This indicates InSAR DEM results are generally slightly lower than real values in the north, and higher in the south; (2) subset B yields a tilt pattern in each pair as well, but the direction is different in the w/ ML pair. For subset B of w/ ML pair (subfigure III and V), the value of difference inclines from east to west, appearing from dark red to dark blue in the images. The w/o ML pairs, on the other hand, resemble subset C, having subtle blue to red coverage from north to south. However, the exception in both situations appears in the north-east hills. The elevation of the hills ranges from 300 to 500 meters, and have negative differences in all pairs. From the color ramp, it is easy to locate the summit of the surrounding; (3) Subset A emerges this same exception more apparently. The elevation summits of subset A, which are located in the northeast and the south, result in negative values in subfigures III, IV, and V, displayed in dark blue. In contrast to the peak areas, other parts of subset A generate large positive values, presenting in dark red. Except subfigure II, which does not share the same background in this case; (4) w/ ML pairs show a distinct characteristic, that the result of difference displays in a more continuous way, while w/o ML pairs appear to be more discrete.

To sum up, in the plane area, the difference tends to incline to one direction, which means generate DEMs by InSAR technique, one side will be higher than true values, and the other side becomes lower. While the elevation surpasses a certain height, the peak of the surrounding yield lower values and the rest would generate higher values.

This phenomenon is in strong contrast in the display, and is more pronounced in w/ ML pairs. This also suggests that elevation has a significant influence on the results.

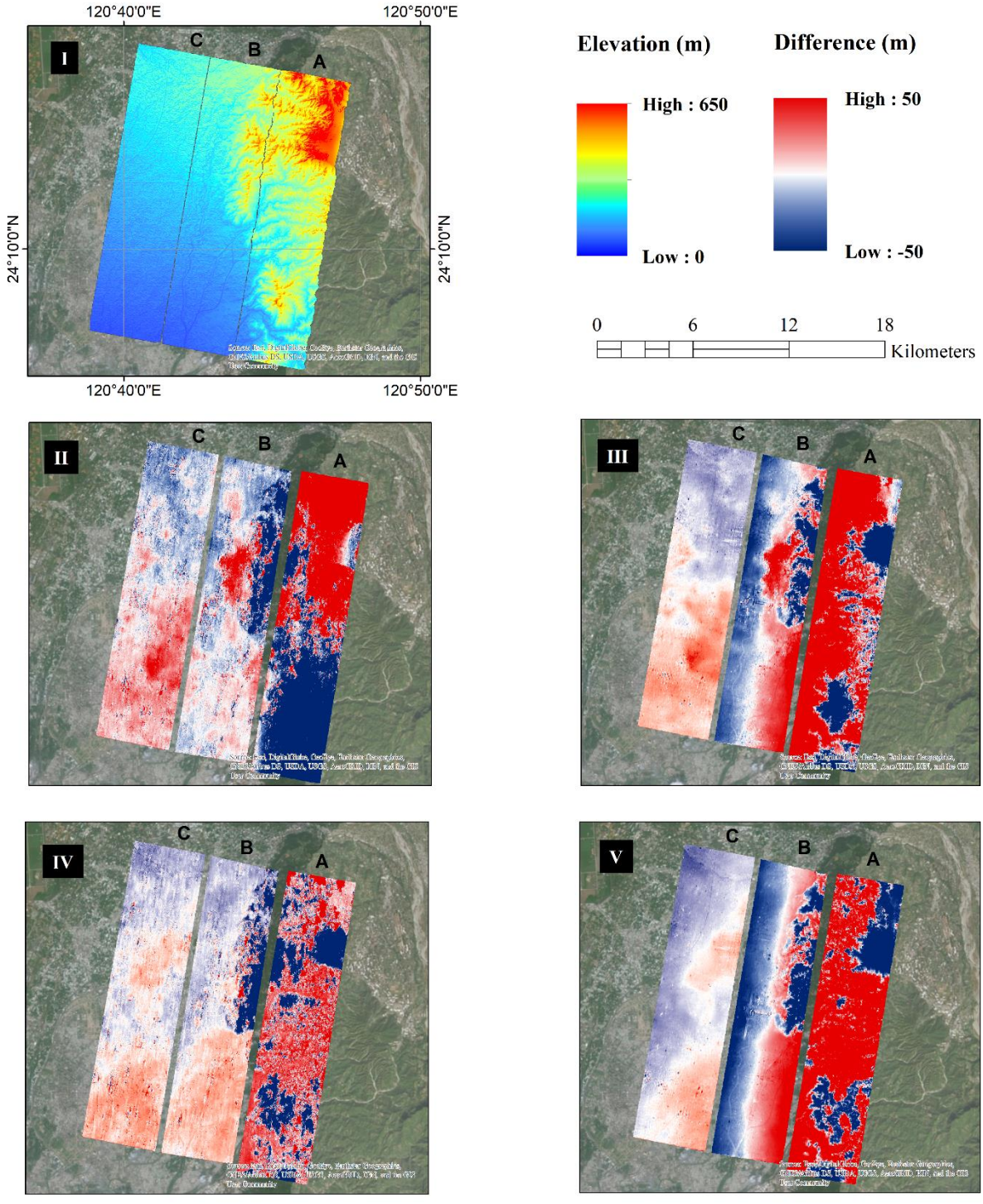

Figure 6 Difference between the InSAR and referenced DEM. Difference results of each pair (subfigure I is a referenced LiDAR DEM, subfigure II is a summer pair w/o ML, subfigure III is a summer pair w/ ML, subfigure IV is a winter pair w/o ML, subfigure V is a winter pair w/ ML)

4.2.2 Quantitative Analysis

In order to conduct further accuracy assessment, 10,000 check points are randomly selected in each subset to calculate Root Mean Square Error (RMSE) for the difference between the InSAR and referenced DEM. The distance between each check point is set to be more than 10 meters. Table 4 displays the statistics information of coherence value, difference and RMSE. Coherence value ranges from 0 to 1, where 0 indicates that the interferometric phase is simply noise, and 1 represents the absence of noise (Ruescas et el. 2009). The coherence value is an important index as it is highly related to temporal stability and phase difference reliability. The higher the coherence value is, the more likely it is to derive useful information (Vasile, 2004).

Table 4 Statistics of coherence values and the result of subtraction

		w/o ML summer			***w/ ML summer***		
		A	B	C	A	B	C
Coherence	min	0.0003	0.0003	0.0001	0.045	0.0493	0.0545
	max	0.9900	0.9928	0.9952	0.986	0.9886	0.9916
	range	0.9897	0.9925	0.9951	0.941	0.9393	0.9371
	mean	**0.3238**	**0.5095**	**0.5659**	**0.3236**	**0.5090**	**0.5560**
	sigma	0.1781	0.2485	0.2368	0.1478	0.2266	0.2127
Difference (m)	min	-648.297	-399.183	-147.506	-387.092	-305.597	-67.771
	max	570.242	283.230	165.489	497.871	136.913	82.328
	range	1218.539	682.413	312.995	884.963	442.51	150.099
	mean	-21.745	-9.351	2.602	58.609	-2.854	2.775
	sigma	**172.752**	**43.132**	**17.831**	**102.843**	**37.403**	**14.636**
RMSE (m)		**172.612**	**43.692**	**18.043**	**118.076**	**37.075**	**14.801**
		w/o ML winter			***w/ ML winter***		
		A	B	C	A	B	C
Coherence	min	0.0003	0.0001	0.0001	0.0495	0.0426	0.0649
	max	0.9953	0.9974	0.9950	0.9930	0.9927	0.9920
	range	0.995	0.9973	0.9949	0.9435	0.9501	0.9271
	mean	**0.3526**	**0.5785**	**0.6659**	**0.3524**	**0.5782**	**0.6659**
	sigma	0.1955	0.2538	0.2135	0.1695	0.2357	0.1926
Difference (m)	min	-321.729	-326.687	-132.778	-231.009	-206.240	-83.631
	max	263.399	292.126	130.165	202.584	123.736	83.934
	range	585.128	618.813	262.943	433.593	329.976	167.565
	mean	0.653	-6.275	2.264	28.852	-7.485	-3.969
	sigma	**57.713**	**34.796**	**13.385**	**65.250**	**36.447**	**12.800**
RMSE (m)		**57.700**	**34.333**	**13.392**	**71.069**	**37.003**	**13.268**

From Table 4, several points could be extracted as follows: (1) within each pair, the higher the coherence value is, the lower the RMSE is; (2) between different pairs, winter pairs have higher coherence value, which leads to better results (smaller RMSE); (3) between different pairs, there is no significant difference in coherence mean between w/ ML pairs and w/o ML pairs, and this property does not relate to RMSE either. However, w/ ML pairs generate better results in summer and worse in winter; (4) the range of coherence is shortened after applying multi-look

processing procedure, thus the sigma of coherence is decreased, but the mean value does not change; (5) along with the change of coherence range, the range of difference values are narrower as well. Nevertheless, this does not influence its mean and sigma.

To conclude, coherence value and the results are strongly related. Seasonal effects directly impact coherence values, and lead to better results for winter pairs over summer pairs. While multi-look processing procedure only decreases the range of coherence, it does not necessary yield a better result in coherence mean. Thus, in the discussion of multi-look processing procedure, the coherence value does not play a role in detecting better results. But we still observe that w/ ML pairs perform better in summer, but worse in winter based on our RMSE statistics.

5. CONCLUSION AND DISCUSSION

This study is based on Sentinel-1A and Sentinel-1B data image processing using the ESA SNAP software package to generate InSAR DEMs. In the research, the influences of seasonal effects and a multi-look processing procedure are the main topics of discussion.

5.1 Seasonal Effect

The analysis has shown that winter data provide better results than summer data. This conclusion is consistent with our previous result. In this study, winter data w/o ML generate the optimal outcome by reaching 13 meters of RMSE, though summer pair could also achieve 15 meters if applying multi-look processing. However, the impact of seasonal effect significantly increases when the elevation is high and when there is more vegetation canopy. Winter pair dataset has reduced RMSE values from 118 meters to 71 meters for w/ ML pair images, and from 173 meters to 57 meters for w/o ML pair images, which indicates that choosing the images based on the season is influential on achieving higher accuracy products, in particular when the area of interest is covered by vegetation and is located at relatively high elevations.

The main factor that contributes to seasonal effects is atmospheric effects. Atmospheric effects happen due to temproal and spatial variations of atmospheric water vapor contents. This causes the loss of coherence and the distortion of phase, and severely compromise the quality of InSAR DEM afterwards (Hanssen, 1998). Hot air during summer days can store more water vapor than cold air, therefore the less humid winter season is more likely to produce good quality outcomes.

5.2 Multi-look Effect

In terms of statistical values, multi-look processing shortens the range of coherence and difference, but this does not necessary lead to a better or worse result. Instead, different seasons show different outcome: w/ ML pair data perform better in summer but worse in winter, which indicates that if summer season pair is needed to be chosen, users could apply multi-look processing during the procedure to mitigate errors. In this study, the influence of conducting multi-look processing is more evident in subset A of summer pair data, which reduces RMSE from 173 meters to 118 meters; in winter pair, multi-look procedures increase RMSE from 58 meters to 71 meters.

The decrease of RMSE can be easily observed in summer pair and high elevation area. One possible reason might be because multi-look processing is helpful to minimize the influence of negative factors, such as atmospheric effects, temporal decorrelation, geometric decorrelation and so on, since this procedure could reduce the noise and increase signal-to-noise ratio. On the other hand, when all of the conditions, like dry weather, feasible baselines, plane terrain etc., are at optimum, applying multi-look processing might only degrade resolution and thus produce lower quality products.

5.3 Further Research

First of all, since there is only one test site in this research, it is feasible to select more areas of interest to test and confirm if the conclusions are empirically supported. Secondly, since terrain height is usually discussed in connection with canopy, it is hard to separate which factor contributes more to the poor result. Therefore, choosing one factor as variable and fix all the others for more InSAR pairs will be further investigated in this research. Thirdly, the optimal look ratio of multi-look processing procedure will also be tested in the future.

6. REFERENCES

ESA, 2019. Radar course 3 (40. Image interpretation: Speckle), Retrieved August 28, 2019, from https://earth.esa.int/web/guest/missions/esa-operational-eo-missions/ers/instruments/sar/applications/radar-courses/content-3/-/asset_publisher/mQ9R7ZVkKg5P/content/radar-course-3-image-interpretation-tone

ESA, 2007, Part B InSAR processing: a pratical approach, Retrieved August 28, 2019, from http://www.esa.int/esapub/tm/tm19/TM-19_ptB.pdf

Hanssen, R.,2001, Radar Interferometry Data Interpretation and Error Analysis, New York, pp. 102-103.

Hanssen, R.,1998, Assessment of the role of atmospheric heterogeneities in ERS tandem SAR interferometry, Report, Delft Inst. Earth-Oriented Space Research, Delft, Netherlands.

Li, F. K., and R. M. Goldstein, 1990, Studies of multibaseline spaceborne interferometric synthetic aperture radars, IEEE Trans. Geosci. Remote Sens., 28(1), pp. 88-97.

Kavzoglu, T., and Saka, M. H., 2005. Modelling local GPS/levelling geoid undulations using artificial neural networks. Journal of Geodesy, Vol. 78, No. 9, pp. 520-527.

Massonnet, D., M. Rossi, C. Carmona, F. Adragna, G. Peltzer, K. Feigl, and T. Rabaute, 1993, The displacement field of the Landers earthquake mapped by radar interferometry, Nature, 364 (6433), pp. 138-142.

Luis Veci, 2016. Sentinel-1 Toolbox TOPS Interferometry Tutorial, Retrieved August 28, 2019, from https://step.esa.int/docs/tutorials/S1TBX%20TOPSAR%20Interferometry%20with%20Sentinel-1%20Tutorial.pdf

Murakami, M., M. Tobita, S. Fujiwara, T. Saito, and H. Masaharu, 1996, Coseismic crustal deformations of 1994 Northridge California earthquake detected by interferometric JERS 1 synthetic aperture radar, Geophysical Research, 101(B4), pp. 8605-8614.

National Development Council, 2016, Ministry of Interior 20-meter grid numerical terrain model data (內政部20公尺網格數值地形模型資料), Retrieved June 1st , 2019, from https://data.gov.tw/dataset/35430

Peltzer, G., and P. Rosen, 1995, Surface displacement of the 17 May 1993 Eureka Valley, California, earthquake observed by SAR interferometry. Science, 268 (5215), pp. 1333-1336.

Rodriguez, E., and J. M. Martin, 1992, Theory and design of interferometric synthetic aperture radars, IEEE Peoceeding, 139(2), pp. 147-159.

UAF, 2018, How to create a DEM from Sentinel-1 Data, Retrieved August 28, 2019, from https://media.asf.alaska.edu/uploads/pdf/current_data_recipe_pdfs/create_a_dem_from_sentinel_1_v1.3.pdf

Vasile, G., Trouve, E., Ciuc, M., Bolon, P. and Buzuloiu, V., 2004. Improving Coherence Estimation f or High-resolution Polarimetric SAR Interferometry. In: Geoscience and Remote sensing symposium, IGARSS '04, Anchorage, USA, Vol. III, pp. 1796-1799.

Wu, Y.Y., Lin, S.Y., 2019, Assessment of interferometric SAR-based digital elevation models. In: International Symposium on Remote Sensing, conference paper #134, Taipei, Taiwan, April 17-19.

Zebker, H. A., and J. Villasenor, 1992, Decorrelation in interferometric radar echoes, IEEE Trans. Geosci. Remote Sens., 30(5), pp. 950-959.

Zebker, H. A., P. A. Rosen, R. M. Goldstein, A. Gabriel, and C. L. Werner, 1994a, On the derivation of coseismic displacement fields using differential radar interferometry: The Landers earthquake, In: Geoscience and Remote sensing symposium, IGARSS '94, Pasadena, USA, pp. 19617-19634.

Zebker, H. A., C. L. Werner, P. L. Rosen, and S. Hensley, 1994b, Accuracy of topographic maps derived from ERS-1 interferometric radar, In: Geoscience and Remote sensing symposium, IGARSS '94, Pasadena, USA, pp. 823-836.